PAPER

Preparation of polypyrrole/titanium nitride composite modified biochar and its application research in microbial fuel cells

Xinyu Jing, Xi Chen, [ID] * Mingchuan Zhang and Xinyang Xu

In this study, the *in situ* growth method was employed to modify biochar with polypyrrole–titanium (PPy–TiN) nitride composites, aiming to enhance its performance as an anode material in microbial fuel cells (MFCs). A series of characterizations were conducted on the polypyrrole-modified corn straw biochar anode (PPy/CS), titanium nitride-modified corn straw biochar anode (TiN/CS), and polypyrrole/titanium nitride composite-modified biochar anode (PPy–TiN/CS) to evaluate the feasibility of the modification method and identify the optimal modification scheme. Characterization techniques included scanning electron microscopy (SEM), Fourier transform infrared spectroscopy (FTIR), electrochemical impedance spectroscopy (EIS), and Tafel analysis. SEM and FTIR analyses confirmed the successful integration of polypyrrole and titanium nitride with biochar, achieving a minimum solution resistance of 7.80 Ω and charge transfer resistance of 1.79 Ω. Compared to the unmodified electrode, the modified electrodes demonstrated improved performance, highlighting the need for the development of cost-effective, efficient, and durable anode materials.

1. Introduction

With the increasing demand for energy and rising pollution emissions, the importance of water quality is reflected across all Sustainable Development Goals (SDGs) outlined by the United Nations.[1] Energy consumption for pollutant removal in waste-water treatment plants accounts for nearly one-third of the operational costs.[2] Microbial fuel cells (MFCs) are a bio-electrochemical device that harnesses the metabolic activity of electrogenic microorganisms to convert organic pollutants in wastewater into electrical energy.[3] Additionally, MFCs facilitate the biodegradation of organic and inorganic compounds, thereby achieving resource recovery and alleviating energy scarcity.[4,5] Significant progress has been made in under-standing microbial electron transfer mechanisms, developing efficient biocatalytic interfaces, and innovating low-cost and durable electrode materials for MFCs.[6] However, the wide-spread adoption of MFCs is hindered by their relatively low power output. The anode material serves as the site for micro-bial adhesion and electron transfer. Additionally, the internal resistance of the anode and the electron transfer resistance between bacteria and the electrode interface directly impact the energy output efficiency of MFCs.[7] Thus, enhancing the power output of MFCs requires the development of cost-effective, readily available, efficient, and durable anode materials.

In recent years, traditional two-dimensional anode carbon materials, such as carbon cloth,[8] carbon paper,[9] carbon felt,[10] graphite rod,[11] graphite fiber brush,[12] and reticulated glass carbon (RVC),[13] have been extensively utilized in MFCs. To enhance the output performance of MFCs, three-dimensional electrodes can theoretically be used to increase the adhesion area of anode microorganisms and the effective area of electron transfer.[14] Common three-dimensional anode materials include graphite particles[15] and granular activated carbon (GAC). Although these materials offer high specific surface area, conductivity, and stability,[16] the production of their raw mate-rials can result in the release of environmental pollutants.[17] Biochar (BC) is a by-product of the thermochemical trans-formation of biomass or its carbonaceous materials.[18] Due to the use of local agricultural and forestry residues as its raw materials, BC has the advantages of wide source, low-cost and recyclable to achieve carbon sequestration.[19] It also has good chemical stability, biocompatibility, and adsorption,[20,21] and can be applied to anodes to improve the electrochemical performance of MFCs. China's total annual straw production accounts for 30% of the world's total production. Direct incin-eration of straw can seriously pollute the environment and cause waste of resources. Corn straw (CS) has high recycling value due to its large amount of nutrients such as cellulose, hemicellulose, and lignin.[22] Murtaza[23] used corn stover biochar to reduce the content of heavy metals in soil biomass. The combination of biochar prepared from waste agricultural corn straw and microbial fuel cell technology to treat pollutants can achieve the purpose of waste recycling and reduction. Thus, this

Northeastern University, No. 11, Lane 3, Wenhua Road, Heping District, Shenyang, China. E-mail: 3036867120@qq.com; 18840622303@163.com; 740148439@qq.com; a18845099174@163.com

study explore the performance of corn straw biochar as an anode for MFCs.

The use of nanocomposites for modification offers an effective approach to optimize electrode of microbial fuel cells (MFCs).[24] Liu et al. enhanced electrical conductivity by fabricating carbon nanotube/polyaniline (CNT/PANI) multilayer membrane composites for MFCs to improve electrochemical performance.[25] Zhao et al. utilized platinum nanoparticles and graphene to synthesize aerogel anodes, thereby enhancing the power density of MFCs.[26] Devasish et al. incorporated polypyrrole and titanium dioxide (PPy/TiO$_2$) nanoparticles at the air–water interface to form nanoparticle composite thin films for the decomposition of organic dyes.[27] Liu et al. loaded polypyrrole (PPy) onto the surface of biochar via chemical oxidative polymerization for use as the anode of MFCs. This modification enhanced the conductivity and capacitance performance of the electrode. Additionally, the positive charge on the electrode surface promoted microbial attachment and electron transfer. As a result, the modified biochar anode achieved a power output 2.5 times higher than that of the unmodified anode.[28] Polypyrrole (PPy) has been widely employed as a conductive polymer material with conjugated double bonds for electrocatalysis and electrochemical electrodes.[29,30] Zou et al. prepared nanostructured polypyrrole anodes for solar microbial fuel cells.[31] However, the electrochemical stability of PPy is limited, and its electrochemical activity is prone to attenuation through oxidation within the electrochemical system. Additionally, PPy exhibits poor biocompatibility, posing challenges for microbial attachment. To enhance the electrochemical stability of polypyrrole electrode materials, researchers have combined them with metal compounds and carbon materials.[32] Transition metal compounds such as nitrides, carbides, and oxides exhibit high electrochemical activity and biocompatibility,[33] facilitating electron transfer between bacteria and electrodes and accelerating biofilm formation. Titanium nitride (TiN), a transition metal nitride, possesses favorable conductivity due to the lower P orbital energy level of nitrogen compared to the Fermi level, and facilitates electron movement within its structure.[34] Moreover, TiN nanopowder demonstrates robust chemical stability and strong adsorption capacity. Li et al. utilized titanium nitride (TiN) alone as the cathode catalyst for MFCs, significantly improving the oxygen reduction reaction (ORR) activity. Higher ORR activity leads to a more efficient cathode reduction reaction, which directly impacts the MFC's output power, efficiency, and stability. The power density of the MFC increased by approximately 40%, demonstrating the excellent catalytic activity and stability of TiN.[35] Combining PPy and TiN in electrode modification for MFCs allows for leveraging the advantageous properties of both materials to achieve electrodes with superior electrochemical performance. Wang et al. combined polypyrrole and titanium nitride for use in supercapacitors and lithium-ion batteries, where the composite exhibited excellent capacitance performance and cycling stability. However, this combination has not been reported in MFC applications. In comparison, this study combines biochar, polypyrrole, and titanium nitride to form a novel composite material, overcoming the limitations of single materials. The composite outperforms single- or dual-component modified materials in terms of conductivity, specific surface area, catalytic activity, and stability. Moreover, the low cost of corn straw biochar, combined with the high catalytic performance of titanium nitride, achieves a balance between high performance and low cost.[36]

In this study, titanium nitride was doped into polypyrrole on corn straw biochar using an in situ growth method to prepare hydrogel electrodes. The prepared PPy–TiN/CS nanocomposite electrodes, along with PPy/CS-modified biochar electrodes, TiN/CS-modified biochar electrodes, and blank control electrodes made of corn straw biochar (CS), were integrated into the system. Following the formation of a stable biofilm on the anode surface, the MFCs underwent electrochemical analysis to explore the power generation, energy storage performance, and pollutant treatment efficacy of the composite anode.

2. Materials and methods

2.1. Preparation of biochar anode

First, the corn straw was crushed and sieved through a 60-mesh sieve. Then, biochar was prepared in a muffle furnace (Shanghai Shengfeng Instrument Equipment Co., Ltd) under a N$_2$ atmosphere through pyrolysis, with a heating rate of 20 °C min^{-1} and a pyrolysis temperature of 800 °C for 2.5 hours to obtain corn straw biochar.[37] The CS biochar was pretreated with mixed acid solution (H$_2$SO$_4$–HNO$_3$) with a volume ratio of 3 : 1 for 45 minutes to promote the formation of the internal pore structure of the biochar. Subsequently, CS biochar was washed several times with deionized water until the residual acid on its surface is completely removed and a neutral pH is reached. The 316 stainless steel mesh purchased from Ning Congsi was utilized as the current collector material to load biochar, with steel wire diameter of 0.3 mm and mesh size of approximately 1 mm. The stainless steel mesh was cut into 7 cm × 7 cm × 1.5 cm rectangular pieces to serve as current collectors. These cut pieces of stainless steel mesh were then subjected to ultrasonic cleaning with acetone (A. R. 99.9%; Tianjin Damao Chemical Reagent Co., Ltd), followed by rinsing with deionized water, and finally dried.

2.2. Preparation of PPy–TiN/CS anode

0.672 mL of pyrrole (A. R. 99.9%; Shanghai Aladdin Biochemical Technology Co., Ltd) monomer, 4.0 mL of isopropanol (A. R. 99.9%; Tianjin Damao Chemical Reagent Co., Ltd), and 1.472 mL of phytic acid (A. R. 99.9%; Shanghai Aladdin Biochemical Technology Co., Ltd) were thoroughly mixed. Then, 0.065 g of titanium nitride (A. R. 99.9%; 20 nm; Shanghai Aladdin Biochemical Science and Technology Co., Ltd) nanopowder was added, and the mixture was uniformly dispersed through ultrasonic agitation. Carbon felt and CS were immersed into this solution, which was then labeled as solution A.

In next step, 2.18 g of ammonium persulfate (A. R. 99.9%; Tianjin Damao Chemical Reagent Co., Ltd) and 0.054 g of carboxymethyl cellulose (A. R. 99.9%; Shanghai Aladdin

Biochemical Technology Co., Ltd) were dissolved in 4 mL of distilled water (solution B). Subsequently, solution A was combined with the solution B in an ice water bath for 50 minutes and allowed to air-dry naturally.

2.3. MFC configuration and operation

Firstly, the Nafion117 proton exchange membrane (Dupont company, USA) was immersed in a 5% H_2O_2 aqueous solution (A. R. 30%; Shanghai Aladdin Biochemical Technology Co., Ltd) at 80 °C for 1 hour. Subsequently, the membrane was thoroughly rinsed with deionized water and soaked in 80 °C deionized water for 1 hour to remove organic impurities and residual H_2O_2. The MFC utilized in the experiment was a rectangular double-chamber reactor constructed from transparent acrylic sheet, with a working volume of 320 mL. The proton exchange membrane separated the cathode and anode chambers, ensuring equal distances between the cathode and anode. Following assembly, the reactor was filled with water and observed for 12 hours for any signs of leakage.

The composition of the synthetic wastewater is as follows: 0.4 g per L CH_3COONa, 0.08 g per L NH_4Cl, 0.08 g per L KCl, 10 mL per L of mineral solution, 4 mL per L of vitamin solution, and 40 mM phosphate buffer solution (PBS). The PBS consists of 2.12 g per L KH_2PO_4, 8.73 g per L $Na_2HPO_4 \cdot 12H_2O$, and 0.4 g per L $NaHCO_3$. The potassium ferricyanide solution consists of 40 mM $K_3[Fe(CN)_6]$ and 40 mM PBS. Prior to inoculation, the anaerobic sludge underwent a pre-treatment process to suppress methanogenic activity, which is crucial for enhancing the performance of microbial fuel cells (MFCs) by promoting the growth of electroactive bacteria over methanogens. The sludge was subjected to a heat treatment at 80 °C for 30 minutes, followed by rapid cooling to room temperature. This process selectively inhibits methanogens, which are more sensitive to heat compared to electroactive bacteria, thereby enriching the sludge with electroactive microorganisms. Additionally, it is important to emphasize that prior to the formal experiments, the activated sludge was pre-cultured in synthetic wastewater for a week. The synthetic wastewater was replaced every three days (the composition of which has been previously outlined) to promote the enrichment of stable electroactive microorganisms in the sludge used for subsequent experiments. Sodium acetate in the synthetic wastewater served as the primary carbon source, providing energy to the microorganisms and preventing their mortality due to nutrient depletion. Subsequently, the anode chamber was inoculated with 80 mL of activated sludge and 170 mL of synthetic wastewater. Following inoculation, the sludge concentration in the anode chamber was 10.8 g L^{-1}. Synthetic wastewater was introduced into the anode chamber, while the cathode chamber was filled with a potassium ferrocyanide solution to serve as the electron acceptor for the cathode. The MFC was then allowed to operate normally and data collection commenced.[38,39]

The MFC was connected to a 1000 Ω external resistor through a data acquisition system (Keithley Instruments Inc., USA), which recorded the voltage data from the external circuit every 0.5 hours. During this process, the anode potential gradually declined, and the MFC voltage output stabilized over time. After 3–4 cycles of reactor operation, microbial stabilization and enrichment on the anode material were achieved. It is also noteworthy that when the MFC's output voltage drops below 100 mV, both the anode solution (synthetic wastewater) and cathode solution should be replaced. A schematic diagram of the microbial fuel cell is provided in Fig. 1.

2.4. Characterization and testing

The linear scanning voltammetry (LSV) curve of different electrodes was measured at a scanning rate of 5 mV s^{-1} by using a three-electrode system in an electrochemical workstation (Chen Hua CHI660D, China) with a scanning range of −0.8–0.8 V. Platinum electrode was used as the counter electrode, saturated calomel electrode was the reference electrode, and modified electrode was the working electrode, respectively. A data
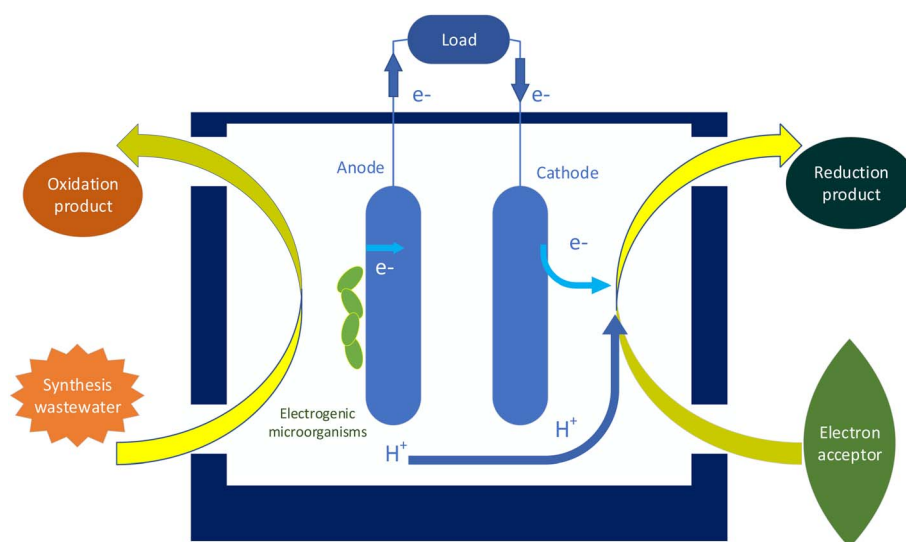

Fig. 1 Schematic diagram of a microbial fuel cell.

acquisition instrument (Agilent 34972A, USA) was used to record the voltage of the MFC every 60 s. The AC impedance spectrum characteristic curve (EIS) was measured in the frequency range of 1 mHz–100 kHz, and the EIS data were fitted by Zview software, the polarization curve and the power density curve were obtained by transforming the external resistance range of 200 Ω–50 kΩ, and the power density was calculated according to the equation

$$P = UI/A \qquad (1)$$

where P is the conversion rate of electrical energy per unit time; U is the difference in potential energy of a unit charge in a circuit; I is the number of charges passing through the conductor section per unit time. The coulombic efficiency (CE) was calculated according to the followed equation[35]

$$CE = \frac{M \int_0^{t_b} I \, dt}{F b v \Delta COD} \qquad (2)$$

where M represents the molecular weight of oxygen, which is taken as 32 g mol^{-1}. The integral of the current I over time from 0 to t_b denotes the total charge passed through the system during this time period. $F \approx 96\,485$ C mol^{-1} is the Faraday constant, representing the charge carried by one mole of electrons. $b = 4$ is the number of electrons exchanged per mole of oxygen. v refers to the volume of the liquid in the anode chamber. ΔCOD represents the change in Chemical Oxygen Demand (COD) over the time interval t_b, indicating the amount of oxygen required for the oxidation of organic matter.

The Japanese Hitachi Regulus 8230 scanning electron microscope (SEM) was used to observe the microscopic surface morphology characteristics within electrodes. The biochar anode was analyzed before and after modification using a Thermo Scientific Nicolet iS20 Fourier transform infrared spectrometer (FTIR).

3. Results and discussion

3.1. Electrode material characterization

Fig. 2 shows the adsorption–desorption pore size distribution of the original material (CS) and the material pretreated with

sulfuric and nitric acid (pretreated CS). The pretreatment with sulfuric and nitric acids effectively removes volatile organic components from the biochar, resulting in significant changes to its pore structure. As shown in the Fig. 2, the pore size distribution of the pretreated material is much richer in the micropore (typically smaller than 2 nm) and mesopore (2–50 nm) ranges, and shows higher adsorption in certain pore size ranges. This phenomenon indicates that the pretreatment process significantly increases the number of micropores and mesopores. This optimization of the pore structure not only improves the specific surface area of the material but also enhances its adsorption capacity for microorganisms and ions. The increase in specific surface area provides more attachment sites for microorganisms, thus promoting microbial adhesion and electron transfer efficiency in microbial fuel cells. In addition, the pretreatment increases the total pore volume of the material, which helps to improve the ion transport rate and, consequently, enhances the electrochemical performance of the material.

Fig. 3 shows the scanning electron microscope analysis of corn straw biochar anode raw materials and their modified composites at 1000–10000 times magnification. A and B are SEM images of CS biochar materials, C and D are SEM images of PPy/CS modified materials, and E and F are SEM images of PPy–TiN/CS composite modified materials.

In Fig. 3B, a considerable number of honeycomb-like cross-sections are evident on the post-pyrolysis biochar materials, showing the relatively uniform sizes of pore structures. The majority of these pores are large, with relatively thin pore wall thickness compared to the diameter of the pores. Furthermore, the concave and convex morphology exhibited on the inner surface of the pores facilitates the attachment of nanoparticles. SEM images of PPy/CS and PPy–TiN/CS at magnifications of 2000× and 5000×, reveal three-dimensional porous structures, indicating that the doping of TiN nanomaterials does not compromise the three-dimensional architecture. Moreover, Fig. 3D illustrates irregular and indefinite stacking of nanoparticles, while Fig. 3F depicts irregular cauliflower-like spherical shapes formed by the aggregation and encapsulation of
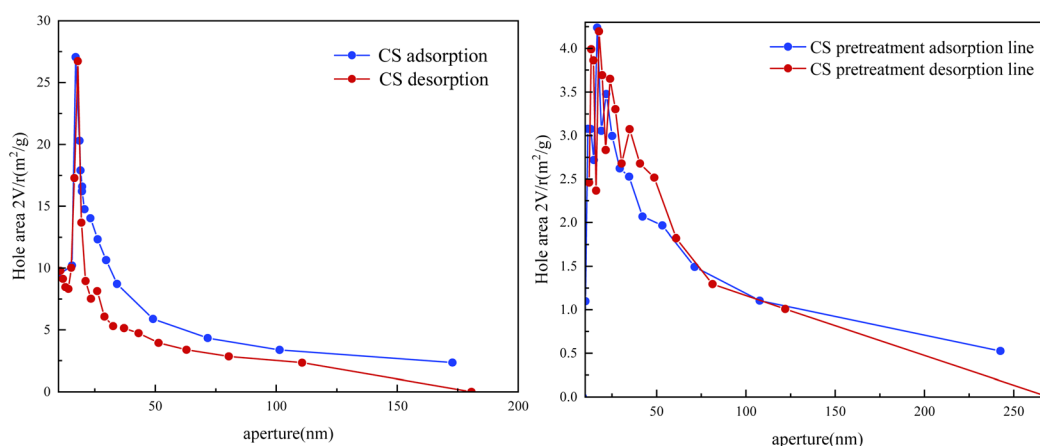

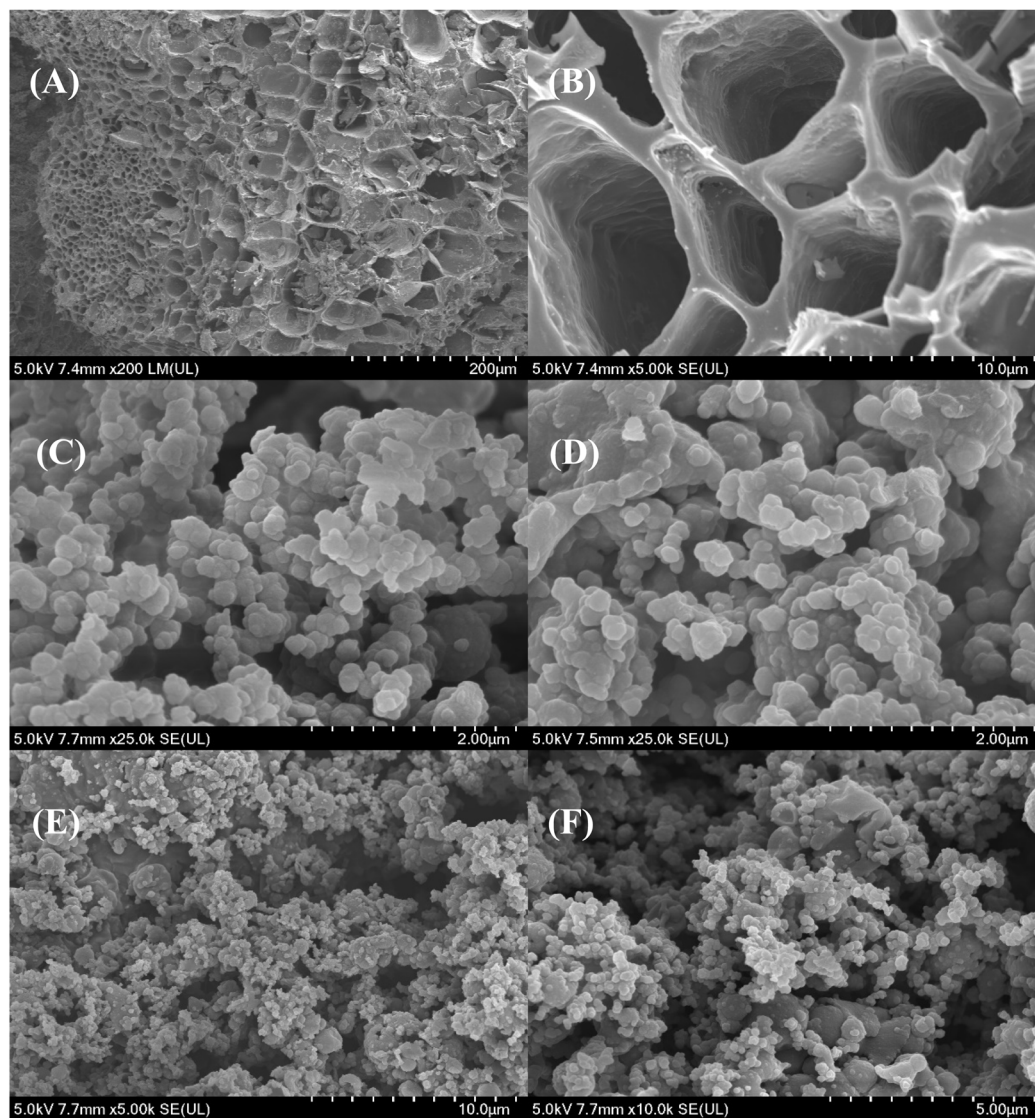**Fig. 2** The adsorption–desorption pore size distribution plot of CS and preprocessed CS.

Fig. 3 Scanning electron microscopy analysis of corn straw biochar anode raw materials and modified composite materials (A and B are SEM images of CS biochar materials, C and D are SEM images of PPy/CS modified materials, and E and F are SEM images of PPy–TiN/CS composite modified materials).

nanoparticles. This suggests that TiN can be uniformly dispersed on the biochar material modified by polypyrrole. Carboxymethyl cellulose, an anionic cellulose possessing biocompatibility, serves to bind, polypyrrole and titanium nitride, together. The three-dimensional porous structure of the corn straw biochar (CS) serves as an ideal scaffold for the PPy–TiN composite, providing a large surface area for microbial colonization. The incorporation of TiN nanoparticles into the PPy matrix not only improves the electrode's conductivity but also enhances its hydrophilicity, which promotes microbial adhesion and biofilm formation. This is supported by the SEM images (Fig. 3), which show a more uniform distribution of nanoparticles on the PPy–TiN/CS surface compared to the PPy/CS electrode. The improved microbial adhesion leads to a more stable and efficient biofilm, which is crucial for sustained electron transfer and power generation in MFCs.

Fig. 4 shows the FTIR spectra of PPy/CS and PPy–TiN/CS composite electrodes. In the PPy/CS infrared spectral curve, the broad peak at $3435~\text{cm}^{-1}$ represents the expansion and contraction vibrations of the OH group. Similarly, in the PPy–TiN/CS IR curve, the peak at $3435~\text{cm}^{-1}$ is shifted to $3127~\text{cm}^{-1}$ and becomes wider. This may be due to the chemical coupling of the alkoxy group and the hydroxyl group in the tetravalent titanium, which shifts the vibrational peak of the hydroxyl group pair towards the lower wavenumber. This interaction suggests a strong chemical bond between PPy and TiN, which stabilizes the composite and enhances its electrochemical performance. The absorption peaked at $1578~\text{cm}^{-1}$ and $1409~\text{cm}^{-1}$ are attributed to the COO^- antisymmetric stretching peak and the $C=C$ symmetric stretching peak, respectively. Additionally, the C–N vibration stretching peaks at $1414~\text{cm}^{-1}$ were characteristic absorption peaks of PPy. The in-plane
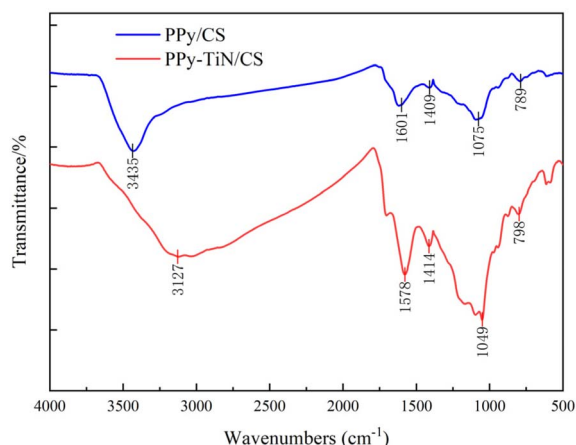
Fig. 4 Infrared absorption spectra of PPy/CS electrode and PPy–TiN/CS electrode.

deformation vibration corresponding to C–H were at 1049 cm^{-1} and 1075 cm^{-1}, as well as peaked at 789 cm^{-1} and 798 cm^{-1} are characteristic absorption peaks of C–H in the α–α connected pyrrole ring β. The peaks at 1578 cm^{-1}, 1414 cm^{-1}, 1075 cm^{-1} and 798 cm^{-1} were distinctive features of PPy and their peak values exhibit changes in functional group energy compared to PPy/CS material. This suggests that the doping of titanium nitride nanoparticles into the ordered nanomixture of polypyrrole induced chemical bond interactions.

XPS measurements were conducted to analyze the elemental composition and chemical states of the PPy/CS and four different doping ratios of PPy–TiN/CS electrodes. C–C/C–H (284.8 eV) corresponds to the sp^2 hybridized carbon atoms in the polypyrrole backbone and the biochar structure. C–N (286.2 eV) indicates the presence of carbon–nitrogen bonds, confirming the successful incorporation of polypyrrole into the

composite. Ti–N (396.8 eV) indicates the formation of titanium nitride (TiN), which is consistent with the successful doping of TiN into the polypyrrole matrix. The O 1s spectrum can be deconvoluted into two peaks: O–Ti (530.2 eV) indicates the presence of titanium oxide (TiO$_2$), which may form due to surface oxidation of TiN during the synthesis process. C=O (531.8 eV) corresponds to oxygen-containing functional groups, such as carbonyl groups, which are consistent with the C 1s spectrum.

The nitrogen content in the PPy–TiN/CS electrode was significantly higher compared to the PPy/CS electrode, confirming the successful modification of the CS biochar electrode surface with PPy and TiN. Both PPy and TiN modifications introduced nitrogen elements. However, with the introduction of PPy, not only was the nitrogen content significantly increased, but the proportion of oxygen was also enhanced. The increased N and O content is beneficial for improving the biocompatibility of the composite material (Fig. 5).

3.2. Electrochemical characterization of different anodes

Fig. 6 shows the LSV scan curves of PPy/CS, TiN/CS, PPy–TiN/CS anode materials, as well as the blank anode control groups of CS and CF. It is evident from Fig. 4 that the current density of the three modified anode materials surpasses that of the two blank control groups, CF and CS. This indicates that the enhancement of power generation performance in the MFC system stems from the anode rather than the cathode. The electrochemical performance of the anode can be assessed by the current density within the voltage range of −0.4 to 0.2 V. According to Fig. 6, it shows that CF (5.95 A m^{-2}) < CS (6.22 A m^{-2}) < TiN/CS (6.59 A m^{-2}) < PPy/CS (7.22 A m^{-2}) < PPy–TiN/CS (8.46 A m^{-2}). It can be concluded that there is a notable increasing trend in current density around 0.03 V, with CS exhibiting a 4.5% increase in current density compared to the blank control CF. This suggests that corn straw biochar possesses superior
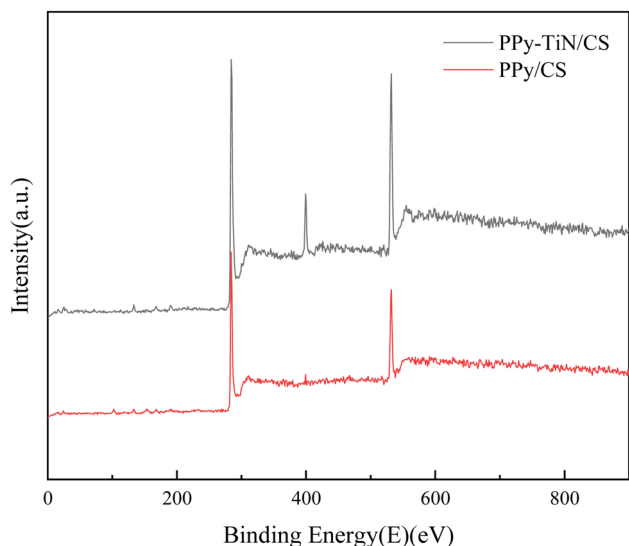

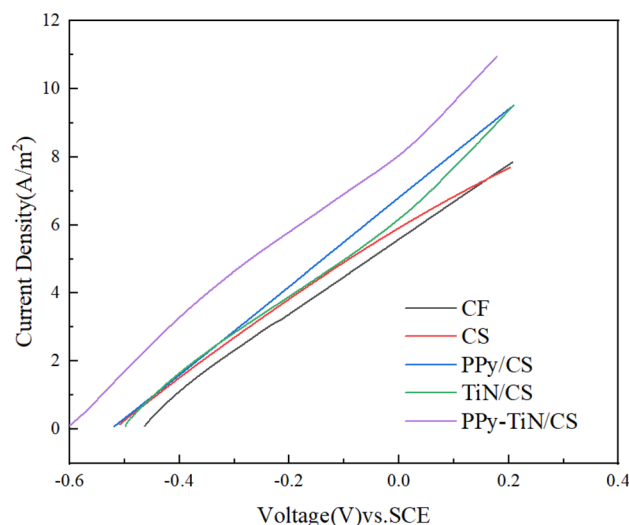**Fig. 5** Infrared absorption spectra of PPy/CS electrode and PPy–TiN/CS electrode.

Fig. 6 LSV scan curves of PPy/CS, TiN/CS, PPy–TiN/CS anode and blank CS and CF anode.
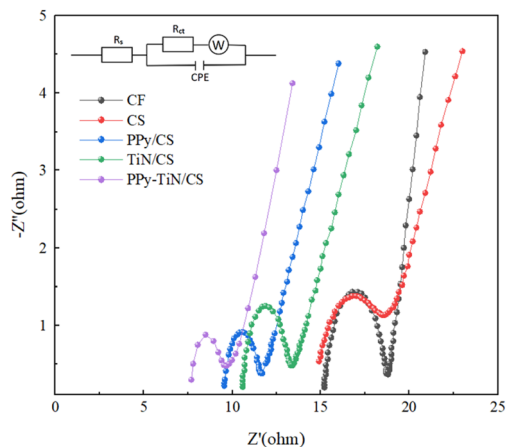
Fig. 7 EIS electrochemical impedance plots of PPy/CS, TiN/CS, PPy–TiN/CS anodes, and CS and CF anodes.

Table 1 Results of EIS fitting data for different anodes

Anode type	CF	CS	TiN/CS	PPy/CS	PPy–TiN/CS
R_s (Ω)	15.14	14.55	9.496	10.58	7.792
R_{ct} (Ω)	3.569	4.121	1.996	2.491	1.794

electrochemical properties compared to the carbon felt blank group due to its porous nature, high specific surface area, and appropriate pore size distribution, enabling efficient electron transport channels.[40]

Furthermore, biochar modification by TiN and PPy results in increases of 5.9% and 16%, respectively, compared to the biochar control. In contrast, the current density of PPy–TiN/CS material experiences a 36% increase compared to CS. From the aforementioned data, it is evident that polypyrrole significantly enhances the conductivity of biochar materials. Although titanium nitride contributes minimally to current density, it exhibits excellent chemical stability and superhydrophobicity. When co-modified with polypyrrole, a synergistic effect arises, combining the stability of both materials with electrochemical activity advantages.

Fig. 7 shows the EIS spectra of different materials in MFCs. By observing the semicircular diameters in the high-frequency region of different anode materials in the Nyquist curve, the charge transfer impedance and electrode reaction kinetic velocity of the modified materials PPy/CS, TiN/CS and PPy–TiN/CS can be analyzed. The resistance parameters solution resistance R_s and charge transfer impedance R_{ct} were quantitatively extracted by fitting the experimental data with the equivalent circuit model diagram, and the fitting results are shown in Table 1.

The R_s values of PPy/CS and TiN/CS were both approximately 27% lower than those of CS. Conversely, the solution resistance of PPy–TiN/CS was notably lower than that of CS, exhibiting a reduction of 46%. This reduction can be attributed to the addition of an effective buffer layer to the electrode post-modification, alongside the highly conductive nature of the

electrode material which mitigates contact resistance between the electrode and the solution. The charge transfer impedance of PPy–TiN/CS is significantly reduced by 49.7% compared to CS. This suggests that PPy–TiN provides a rich porous structure for the biochar material, offering good selectivity and stability. The three-dimensional porous structure of corn straw biochar serves as a stable framework for this modification method, ensuring full contact with the electrolyte to facilitate ion transfer and transportation. When PPy and TiN are combined, the resulting composite material benefits from the complementary properties of both components. The PPy provides a conductive matrix that facilitates electron transfer, while the TiN nanoparticles enhance the stability and biocompatibility of the electrode. This synergistic effect is evident in the reduced charge transfer resistance (R_{ct}) and solution resistance (R_s) observed in the PPy–TiN/CS composite, as shown in Table 1. The R_{ct} of PPy–TiN/CS (1.794 Ω) is significantly lower than that of PPy/CS (2.491 Ω) and TiN/CS (1.996 Ω), indicating that the composite material provides a more efficient pathway for electron transfer.

3.3. Tafel curve

Fig. 8 illustrates the Tafel electrochemical test plot of the modified biochar anode alongside the blank control anode. The Tafel slope was determined by measuring the voltage–current curve of the MFC under varying loads, enabling evaluation of the kinetic characteristics of the electrode reaction. A smaller slope indicates faster reaction kinetics of the electrode and enhanced battery power production. By extrapolating the linear region on the extension curve, the intersection value with the ordinate yields the logarithm of the exchange current density.

Subsequently, the anode's current density (i_0) can be derived by taking the logarithm of this value, as shown in Table 2 below. The relationship between the AC current density of the anode is as follows: CF < CS < PPy/CS < TiN/CS < PPy–TiN/CS. Higher AC current density corresponds to increased electron transfer efficiency and faster reaction kinetics on the electrode surface. Notably, the reaction rate of the PPy–TiN/CS anode surface is
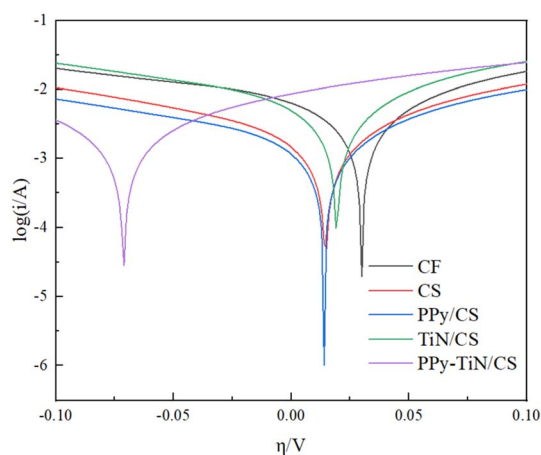

Fig. 8 Tafel curves for different anodes.

Table 2 Linear fitting equation and AC current density i_0 for the straight part of the Tafel curve

The anode electrode	Linear fitting equation	$i_0 \times 10^{-3}$ (A cm^{-2})
CF	$Y = 5.6582x - 3.1642$	0.6852
CS	$Y = 5.7922x - 2.9583$	1.1008
PPy/CS	$Y = 4.1558x - 2.7247$	1.8850
TiN/CS	$Y = 4.8961x - 2.8565$	1.3916
PPy–TiN/CS	$Y = 4.6472x - 2.4387$	3.6417

the highest, with a significantly higher AC current density compared to the blank group CS. The enhanced performance of the PPy–TiN/CS composite can be further explained by the formation of a conductive network within the biochar matrix. The PPy chains create a continuous conductive pathway, while the TiN nanoparticles act as electron transfer mediators, reducing the energy barrier for electron transfer between the bacteria and the electrode. This is supported by the Tafel analysis (Fig. 8), which shows that the PPy–TiN/CS electrode has the highest exchange current density ($i_0 = 3.6417$ A cm^{-2}), indicating faster reaction kinetics and more efficient electron transfer compared to the individually modified electrodes.

3.4. Analysis of MFC power production performance

Fig. 9 depicts the output voltage over time during the stable operation period of the MFC using various anode materials. It is evident that the maximum stable output voltage value observed with PPy and TiN modified CS is notably higher than that of the other groups, aligning with the analysis results from the preceding electrochemical test section. Specifically, the maximum output voltage recorded for PPy–TiN/CS during reactor operation is 653 mV, representing an increase of 5.1%, 7.2%, 5.6%, and 5.3% compared to CS, CF, PPy/CS, and TiN/CS materials, respectively.

Fig. 10 illustrates the power density curves of different anodes following stable operation of the MFC. These curves
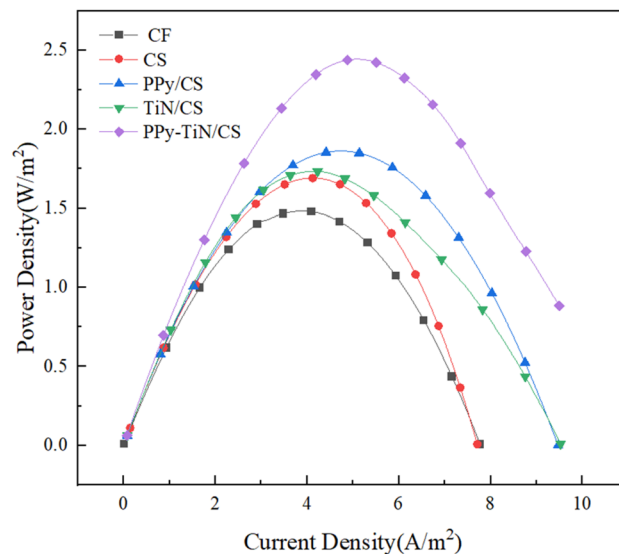

Fig. 9 Output voltage curves for different anodes.

Fig. 10 Power density curves for different anodes.

depict the variation in output power of the MFC under various external resistance loads, with the maximum power point (PPP) being a crucial feature indicating the point at which $P = UI$ reaches its peak value, thereby reflecting the power production performance of the microbial fuel cell. According to the power density curve, the maximum power densities of CF, CS, PPy/CS, TiN/CS, and PPy–TiN/CS are 1.48 W m^{-2}, 1.69 W m^{-2}, 1.73 W m^{-2}, 2.44 W m^{-2}, and 2.86 W m^{-2}, respectively. The order of power densities is CF < CS < PPy/CS < TiN/CS < PPy–TiN/CS, indicating that the power production performance of the MFC is influenced by the biochar modification method. PPy–TiN/CS demonstrates a 64.8% increase compared to unmodified CS, suggesting that the combined modification of polypyrrole and titanium nitride maximizes the electrode efficiency of biochar. This result is consistent with the findings of LSV, EIS, and Tafel's test. In recent studies, the modification of biochar with conductive polymers such as polypyrrole (PPy) has been shown to improve the electrochemical performance of the material due to enhanced conductivity and structural stability. For instance, Zhang et al. (2020) demonstrated that PPy-modified biochar materials significantly improved charge transfer rates and capacitance due to the uniform distribution of PPy on the biochar surface. However, while PPy alone enhances conductivity, it may not fully exploit the potential of biochar's porous structure. Introducing titanium nitride (TiN) into the composite material, as observed in our study, offers additional benefits. TiN has been widely recognized for its high electrical conductivity, thermal stability, and catalytic properties.[41] When combined with PPy, TiN not only contributes to the overall conductivity but also aids in the uniform dispersion of nanoparticles, which can further enhance the material's electrochemical performance.

Fig. 11 illustrates the polarization curves of different anodes following stable operation of the MFC. The polarization curve elucidates the relationship between output voltage and current
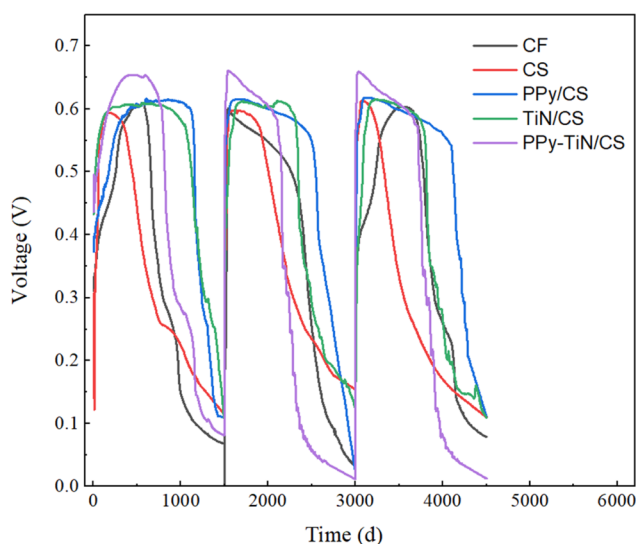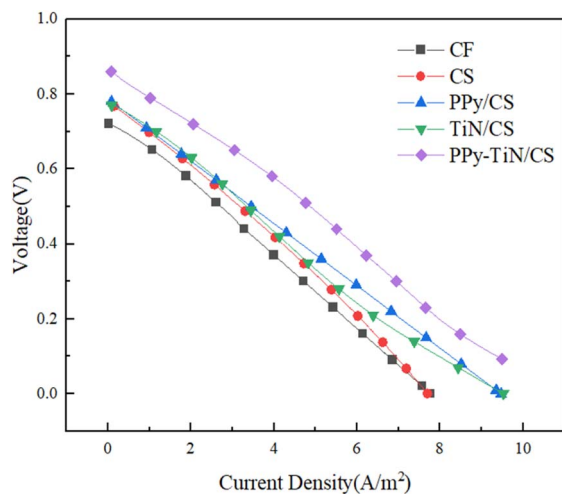
Fig. 11 Polarization curves for different anodes.

Fig. 12 COD removal rate *vs.* coulombic efficiency CE for different anodes.

compared to other electrode materials, followed by PPy/CS. This suggests that biochar materials modified solely by titanium nitride and polypyrrole have a limited effect. Conversely, the successful modification of PPy–TiN/CS anode materials showcases excellent power production performance. Observing the polarization curve, the polarization improvement effect of titanium nitride doping and polypyrrole modification alone appears inconspicuous. This is attributed to the fact that PPy undergoes expansion or contraction during MFC charging and discharging, compromising cell stability and cyclability.[42] The incorporation of doped titanium nitride nanomaterials theoretically enhances electrode superhydrophobicity and stability, facilitating the formation of a porous nanostructure. The synergistic performance of these materials enables the electrode to exhibit robust anti-polarization properties.

Fig. 12 presents the COD removal rate and coulombic efficiency of different anodes during MFC operation. It is evident that the COD removal rate of the material modified with polypyrrole and titanium nitride is 23.9% higher than that of the control group CS. Conversely, the microbial removal efficacy of the two separately modified materials is suboptimal. Additionally, the coulombic efficiency (CE) of PPy–TiN/CS exhibited the highest value within the group at 55.6%, surpassing CF, CS, PPy/CS, and TiN/CS by 58%, 43.9%, 20.6%, and 39.9%, respectively. To validate the high CE value, we cross-reference our results with other studies that have reported similarly high CE values using advanced anode materials. Lv *et al.*[43] reported a CE of 52% for polypyrrole/graphene oxide composites used in MFCs. This value is close to the 55.6% achieved by our PPy–TiN/CS composite anode, indicating that the incorporation of conductive polymers with metal-based materials can significantly enhance CE. Liu *et al.*[44] demonstrated a CE of 50% using CNT/PANI multilayer membrane composites. This further supports the notion that composite materials combining conductive polymers with nanostructured additives can achieve high CE values. Zhao *et al.*[45] reported a CE of 48% for three-dimensional graphene/Pt nanoparticle composites. While slightly lower than our value, it still indicates that advanced composite materials can achieve high CE values.

To substantiate the claim of "superior performance" of the PPy–TiN/CS composite anode, we compare its electrochemical performance with several state-of-the-art anode materials reported in recent literature. The key performance metrics, such as power density, current density, and charge transfer resistance, are summarized in Table 3.

under varying external resistance conditions, indicating that the MFC exhibits higher voltage output when internal resistance is lower, given the same current. As depicted in the power density curve, the output voltage and current density exhibit a linear relationship, signifying the stability of the microbial fuel cell operation. Notably, with increasing current density, PPy–TiN/CS demonstrates the lowest degree of polarization

Table 3 Comparison of PPy–TiN/CS composite anode with state-of-the-art anode materials

Anode material	Power density (W m^{-2})	Current density (A m^{-2})	Charge transfer resistance (Ω)	Coulombic efficiency (%)	Reference
PPy–TiN/CS composite	2.86	8.46	1.794	55.6	This study
Graphene/Pt nanoparticles	2.1	7.5	2.0	50.0	Zhao *et al.*[45]
CNT/PANI composites	1.8	6.8	2.5	45.0	Liu *et al.*[46]
PPy/TiO$_2$ composites	1.5	6.0	3.0	40.0	Devasish *et al.*[47]
Graphene-modified biochar	1.9	7.0	2.2	48.0	Zheng *et al.*[48]
Activated carbon (AC)	1.2	5.5	3.5	35.0	Huggins *et al.*[49]

4. Conclusions

In this study, a novel porous nano-biochar electrode was successfully prepared using an *in situ* growth method, characterized by a high specific surface area, excellent conductivity, good biocompatibility, and stability. This electrode material was employed in microbial fuel cells (MFCs), and the properties of three modified materials (PPy/CS, TiN/CS, PPy–TiN/CS) and two control groups were analyzed. Notably, the modified PPy–TiN/CS anode exhibited outstanding electrochemical performance, with a maximum output voltage of 653 mV, maximum power density of 2.44 W m^{-2}, current density (i_0) of 3.64 A m^{-2}, and coulombic efficiency (CE) of 55.6% during stable MFC operation. These results demonstrate that the composite modification of polypyrrole and titanium nitride offers an effective approach to enhancing the energy yield of MFCs, facilitating suitable electron exchange transport space, and achieving efficient electron transfer. Moreover, considering the low cost and sustainability of biochar, combined with the excellent performance of the PPy–TiN/CS composite anode, it demonstrates its potential for large-scale applications in wastewater treatment and sustainable energy production, providing valuable insights for the future design of advanced electrode materials in this field.

In summary, the success of the PPy–TiN/CS composite in enhancing MFC performance highlights the potential of combining conductive polymers with metal-based materials for the development of high-performance, low-cost electrodes. Future research could explore the use of other transition metal nitrides or carbides in combination with conductive polymers to further optimize the electrochemical properties of biochar-based electrodes. Additionally, the long-term stability and scalability of these composite materials should be investigated to assess their feasibility for large-scale MFC applications.

Data availability

The data that support the findings of this study are available from the corresponding author upon reasonable request.

Conflicts of interest

There are no conflicts to declare.

References

1 N. Subran and K. Ajit, Synthesis and performance of a cathode catalyst derived from areca nut husk in microbial fuel cell, *Chemosphere*, 2023, **312**, 137303.

2 J.-H. Hwang and H. Ryu, A strategy for power generation from bilgewater using a photosynthetic microalgal fuel cell (MAFC), *J. Power Sources*, 2021, **484**, 229222.

3 P. Pandey and V. N. Shinde, Recent advances in the use of different substrates in microbial fuel cells toward wastewater treatment and simultaneous energy recovery, *Appl. Energy*, 2016, **168**, 706–723.

4 N. A. Logan, B. E. Rabaey and J. M. S. Harnisch, Microbial fuel cells: A new frontier in energy generation and waste treatment, *Trends Biotechnol.*, 2006, **24**, 452–460.

5 A. Dumitru and K. Scott, 4 - Anode materials for microbial fuel cells, *Microbial Electrochemical and Fuel Cells*, 2016, pp. 117–152.

6 C. Santoro and C. Arbizzani, Microbial fuel cells: From fundamentals to applications, *J. Power Sources*, 2017, **356**, 225–244.

7 J. Zhao and J. Wang, Novel method for preparation of metal-sulfide@reduced-graphene-oxide with high energy storage performance, *Mater. Chem. Phys.*, 2020, **240**, 122132.

8 S. M. Strycharz and A. P. Malanoski, Application of cyclic voltammetry to investigate enhanced catalytic current generation by biofilm-modified anodes of Geobacter sulfurreducens strain DL1 vs. variant strain KN400, *Energy Environ. Sci.*, 2011, **4**(3), 896–913.

9 J. R. Kim and S. H. Jung, Electricity generation and microbial community analysis of alcohol powered microbial fuel cells, *Bioresour. Technol.*, 2007, **98**(13), 2568–2577.

10 H. J. Kim and H. S. Park, A mediator-less microbial fuel cell using a metal reducing bacterium, Shewanella putrefaciens, *Enzyme Microb. Technol.*, 2002, **30**(2), 145–152.

11 B. Logan, Power generation in fed-batch microbial fuel cells as a function of ionic strength, temperature, and reactor configuration, *Environ. Sci. Technol.*, 2005, **39**(14), 5488–5493.

12 H. Zhang and C. Chen, Effect of feedstock and pyrolysis temperature on properties of biochar governing end use efficacy, *Biomass Bioenergy*, 2017, **105**, 136–146.

13 Z. He and N. Wagner, Electricity generation from artificial wastewater using an upflow microbial fuel cell, *Environ. Sci. Technol.*, 2005, **39**(14), 5262–5267.

14 K. You and Z. Zhou, *Preparation of Biochar-based Electrode and its Bioelectrochemical Application*, MDPI, 2021, vol. 11, 4, p. 508.

15 S. You and Q. Zhao, A graphite-granule membrane-less tubular air-cathode microbial fuel cell for power generation under continuously operational conditions, *J. Power Sources*, 2007, **173**(1), 172–177.

16 W. Jincheng, P. Liang and X. Huang, Recent progress in electrodes for microbial fuel cells, *Bioresour. Technol.*, 2011, **102**(20), 9335–9344.

17 H. Tyler and H. Wang, Biochar as a sustainable electrode material for electricity production in microbial fuel cells, *Bioresour. Technol.*, 2014, **157**, 114–119.

18 N. Yang and H. Luo, Three-dimensional electrodes enhance the power generation and denitrification capacity of microbial fuel cells Bioprocess and Biosystems Engineering, *Bioresour. Technol.*, 2023, 129026.

19 J. Lehmann, A handful of carbon, *Nature*, 2007, **447**(7141), 143–144.

20 M. Ghasemi, Nano-structured carbon as electrode material in microbial fuel cells: A comprehensive review, *J. Alloys Compd.*, 2013, **580**, 245–255.

21 Y. Gao and Y. Zhang, Facile synthesis of high-surface area mesoporous biochar for energy storage via in-situ template strategy, *Mater. Lett.*, 2018, **230**, 183–186.

22 F. Suo and X. You, Preparation and characterization of biochar from modified corn straw and its potential as a soil amendment, *Biol. Resour.*, 2021, 149167.

23 G. Murtaza, Effectiveness of corn stalk biochar in amending the contaminated soil attributes and enhancing the sustainable grass growth, *Global NEST J.*, 2024, **26**(01), 5429.

24 S. Zhang, Graphene-modified biochar anode on the electrical performance of MFC, *Ferroelectrics*, 2021, **578**(1), 1–14.

25 Q. Liu and Y. Yang, Properties of Polyaniline/Carbon Nanotube Multilayer Films in Neutral Solution and Their Application for Stable Low-Potential Detection of Reduced β-Nicotinamide Adenine Dinucleotide, *Langmuir*, 2010, **26**, 1286–1292.

26 S. Zhao and Y. Li, Three-dimensional graphene/Pt nanoparticle composites as freestanding anode for enhancing performance of microbial fuel cells, *Sci. Adv.*, 2015, **1**(10), e1500372.

27 D. Chowdhury and A. Paul, *Photocatalytic polypyrrole-TiO2-nanoparticles composite thin film generated at the air-water interface*, *Surf. Colloids*, 2005, **21**(9), 4123–4128.

28 X. Liu and D. Zhang, Polypyrrole-coated biochar as a high-performance anode material for microbial fuel cells, *J. Power Sources*, 2017, **358**, 39–46.

29 G. Han, Electrodeposition of polypyrrole/multiwalled carbon nanotube composite films, *Thin Solid Films*, 2005, **474**, 64–69.

30 Y. Chen and W. Zhang, Characterization and research Progress of Conductive Polymer Nanomaterials, *Energy Storage*, 2004, **101**, 113813.

31 Y. Zou and J. Pisciotta, Nanostructured polypyrrole-coated anode for sun-powered microbial fuel cells, *Bioelectrochemistry*, 2010, **79**(1), 50–56.

32 Z. Lv and Y. Chen, One-step electrosynthesis of polypyrrole/graphene oxide composites for microbial fuel cell application, *Electrochim. Acta*, 2013, **111**, 366–373.

33 M. Yu, Holey tungsten nitride nanowires: a novel anode that efficiently integrates microbial chemical energy conversion and electrochemical energy storage, *Adv. Mater.*, 2021, **33**(39), 2102551.

34 M. Q. Snyder and S. A. Trebukhova, Synthesis and characterization of atomic layer deposited titanium nitride thin films on lithium titanate spinel powder as a lithium-ion battery anode, *J. Power Sources*, 2007, **165**(1), 379–385.

35 X. Li, Titanium nitride catalyst cathode in a Li-air fuel cell with an acidic aqueous solution, *Mater. Chem. A*, 2016, **11**, 4177–4185.

36 Y. Wang and M. Zhang, A Biochar/Polypyrrole/Titanium Nitride Composite for High-Performance Electrocatalysis and Energy Storage, *Mater. Chem. A*, 2020, **8**, 9022–9031.

37 Z. Wang and Z. Tan, Direct current electrochemical method for removal and recovery of heavy metals from water using straw biochar electrode, *Cleaner Prod.*, 2022, **339**, 130746.

38 B. E. Logan, Microbial Fuel Cells: Methodology and Technology, *Environ. Sci. Technol.*, 2006, **40**(17), 5181–5192.

39 J. R. Kim, Electricity generation and microbial community analysis of alcohol-powered microbial fuel cells, *Bioresour. Technol.*, 2007, **98**(13), 2568–2577.

40 X. Wu, Preparation of C@PPy/TiN nanocomposite with excellent cycling stability via a one-step hydrothermal method, *Ceram. Int.*, 2016, **42**(13), 15077–15080.

41 Y. Li and X. Zhang, Titanium Nitride as a Catalytic and Conductive Material for Energy Applications, *Mater. Chem. A*, 2017, **5**, 873–883.

42 L. Wang and J. Zhao, Enhanced Performance of PPy-TiN/CS Anodes for Microbial Fuel Cells: Investigation of Polarization Behavior and Stability, *Electrochim. Acta*, 2021, **372**, 1378–1386.

43 L. Zhisheng and C. Yanfeng, One-step electrosynthesis of polypyrrole/graphene oxide composites for microbial fuel cell application, *Electrochim. Acta*, 2013, **111**, 366–373.

44 H. Liu and S. A. Cheng, Power generation in microbial fuel cells using carbon nanotube/PANI composites as electrodes, *Electrochem. Commun.*, 2011, **13**, 59–62.

45 F. Zhao and W. Dong, three-dimensional graphene/Pt nanoparticle composites for efficient microbial fuel cell electrodes, *J. Mater. Chem. A*, 2015, **3**(17), 8919–8926.

46 H. Liu and S. A. Cheng, Power generation in microbial fuel cells using carbon nanotube/PANI composites as electrodes, *Electrochem. Commun.*, 2011, **13**(1), 59–62.

47 D. Chowdhury and A. Paul, *Photocatalytic Polypyrrole-TiO$_2$-Nanoparticles Composite Thin Film Generated at the Air–Water Interface*, PMID, 2005, **21**, 4123–4128.

48 Z. Fang and W. Lin, Large-flake graphene-modified biochar for the removal of bisphenol S from water: rapid oxygen escape mechanism for synthesis and improved adsorption performance, *Environ. Pollut.*, 2023, **317**, 120847.

49 T. Huggins, Wang, *Biochar as a sustainable electrode material for electricity production in microbial fuel cells*, *Bioresour. Technol.*, 2014, **157**, 114–119.